Infrared Physics and Technology 93 (2018) 63–69

Contents lists available at ScienceDirect

Infrared Physics & Technology

journal homepage: www.elsevier.com/locate/infrared

Regular article

# Influence of image resolution on the performance of remote breathing rate measurement using thermal imaging technique

Menghan Hu, Guangtao Zhai*, Duo Li, Hanqi Li, Mengxin Liu, Wencheng Tang, Yuanchun Chen

*Institute of Image Communication and Information Processing, Shanghai Jiao Tong University, Shanghai 200240, PR China*

ARTICLE INFO

*Keywords:*
Thermal imaging
Influence of resolution
Respiration measurement
Non-contact techniques

ABSTRACT

The aim of this work was to evaluate the influence of a thermal image resolution on the performance of thermal imaging system for remote and unobtrusive breathing rate (BR) measurement. The thermal imager with original resolution of 640 × 480 was first used to establish the thermal imaging system. The thermal video database containing 60 videos was developed to validate the feasibility of this system for BR measurement. Subsequently, the nearest-neighbor interpolation was exerted to create the thermal videos with low resolutions. The Bland-Altman plots of BR showed that distances between the upper and lower 95% limits of agreements were 4.094 bpm, 10.595 bpm, 10.091 bpm, 15.168 bpm and 20.769 bpm for video resolutions of 640 × 480, 512 × 384, 320 × 240, 192 × 144 and 64 × 48, respectively. With respect to linear regression analysis, the determination coefficient ($R^2$) of 0.898, 0.890, 0.900, 0.776 and 0.539 had been found for the resolutions of 640 × 480, 512 × 384, 320 × 240, 192 × 144 and 64 × 48, respectively. These two statistical approaches both demonstrated that the thermal resolution of 320 × 240 achieved the performance comparable to the high thermal resolution. Inspired by the above results, for the practical applications, we can choose the appropriate resolution by taking both the system performance and cost into account. In this case, the thermal video resolution of 320 × 240 could be selected for BR measurement in some application scenarios (i.e. lie detection) where the measurement distance is approximately 1.5 m. This research may greatly improve the design of the contactless measurement device for physiological signals.

## 1. Introduction

Breathing rate, one of the four main vital physiological signals, is the measure of basic body functions [1]. The abnormal breathing rate always provides potential clues for many diseases. For example, the increase in breathing rate may forebode the occurrence of hypoxaemia or hypercarbia [2]. Hence, breathing rate is regarded as an important predictor of serious illnesses. Numerous existing non-invasive measurement techniques such as electrical impedance tomography [3] can estimate breathing rate in contact way. The contact measurement approaches require some cumbersome sensors to be attached on the body, and therefore, they are not in general well tolerated by most users. Luckily, non-contact techniques can offer a comfortable way of measuring breathing rate.

For contactless measurements, the radar methods take advantage of Doppler phenomenon to detect chest movements caused by breathing. Nahar et al., developed the radar sensing system for estimating the breathing rate of the human subject behind the wall [4]. Ultrasound methods also utilize the Doppler effect to measure breathing rate. The viability of ultrasonic devices for breathing measurements has been investigated by many researchers [5,6]. However, these two sensors have the potential radiation hazards [7]. We can also derive the breathing rate using video data via the analysis of movement variation [8]. Shao et al., extracted the breathing signal hiding in a small movement of shoulders [9]. Nonetheless, the video-based methods are in nature sensitive to illumination changes. To solve this shortcoming, Aoki et al., projected the infrared light array on the chest of the subject, and then the breathing rate could be determined by calculating relative positions of infrared light spots [10]. Although numerous attempts have been made to improve the abovementioned approaches, their detection accuracies are still highly dependent on the motion artefact [11].

In contrast to the active sensor devices, the passive thermal imaging can collect the emitted energy from the objects whose absolute temperature is higher than zero without any external stimulation such as harmful radiation and illumination [20]. Table 1 presents the summary of commonly used sensors for the unwired and unobtrusive breathing rate measurement. A thermal camera is a device that gives an image using infrared radiation in wavelengths as long as 14 μm, like an RGB

* Corresponding author.
*E-mail address:* zhaiguangtao@sjtu.edu.cn (G. Zhai).

https://doi.org/10.1016/j.infrared.2018.05.026
Received 13 March 2018; Received in revised form 24 May 2018; Accepted 29 May 2018
Available online 30 May 2018
1350-4495/ 

**Table 1**
Summary of commonly used sensors for the unwired and unobtrusive breathing rate measurement.

| Sensor | Principle | Advantage | Disadvantage | Some current literature |
|---|---|---|---|---|
| Doppler radar | Measure chest wall motion | Through-clothing and through wall breathing evaluation | "Potential" radiation* and high sensitivity to motion artifacts | Nahar et al. [4] Droitcour et al. [12] |
| Laser Doppler vibrometer | Estimate chest wall velocity and displacement | No electric, radiation and biological risks | High sensitivity to selected points on the thoracic surface | Scalise et al. [13] |
| Ultrasonic proximity sensor | Compute time intervals between transmitted and received sound waves | Through-clothing breathing evaluation and no biological risk | High sensitivity to motion artifacts | Min et al. [6] Arlotto et al. [5] |
| Visible imaging sensor | Detect and analyze the body movement | Easy and burden-free measurement | High dependence on slight movements | Shao et al. [9] Reyes et al. [14] Nam et al. [15] |
| Microsoft Kinect sensor | Capture depth maps using Time of Flight technology | Easy and inexpensive measurement | High influence by some obstructions such as cloths and blankets | Centonze et al. [16] Lee et al. [17] |
| Thermal imagery | Record the object's emitted energy and calculate temperature changes around nostrils or mouth | Illumination and movement independence | Absence of geometric and textural details in obtained image sequences | Basu et al. [18] Hu et al. [19] |

* Note: since the low-power radar can measure BR, the potential radiation maybe minimal if it exist. However, the majority of people may still consider subconsciously that the radar is radioactive.

camera in the mobile phone that gives an image using visible light in wavelengths from 400 to 700 nm. In this sense, the obtained thermal images are illumination-independent. The sequential thermal images can give the heat map series as a function of time in the region of interest (ROI). From these heat distributions, temperature variations in nostrils and mouth regions, which accompany the inhalation and exhalation, can be extracted for the determination of breathing rate irrespective of changes in position or illumination intensity [18,21]. Pereira et al., acquired the great agreement between the estimated breathing rate using the thermal imaging technique and ground truth with the 95% limits of agreement ranging from −1.4 bpm to 1.3 bpm [22]. Similar results were also obtained by other groups of investigators [23–25]. Nevertheless, the aforementioned researches used thermal imager with high resolution such as 1024 × 768 pixels and 1600 × 1200 pixels or relatively low resolution such as 320 × 240 pixels with a very close testing distance. With respect to the practical applications, it is necessary to balance the system cost (increase with the camera resolution) and its performance. Bai et al., discussed the measuring sensitivity in respect to the detection distance, and no detailed experimental results were available in their study [26]. The key differences between some previous studies are summarized in Table 2. From Table 2, we can preliminarily conclude that there is no unified standard for us to select a suitable thermal camera for the design of breathing rate measurement device (different investigators used different imaging hardware configurations). Also, in their studies, the accuracies of systems are all stated to be acceptable. Hence, the influence of image resolution on accuracy of breathing rate measurement is urgent to be studied.

The objectives of the current study are to: (1) establish a thermal imaging system and acquire a thermal video with different resolutions; (2) construct a database to validate the performances of the thermal imaging system and the corresponding algorithm; and (3) analyze the influence of image resolution on the accuracy of remote breathing rate measurement.

## 2. Methods

### 2.1. Thermal imaging system

Fig. 1 shows the experimental setup. A thermal imager (MAG62, Magnity Electronics Co. Ltd., Shanghai, China) with the resolution of 640 × 480 is placed on a tripod to avoid vibration during the experiments. The pixel pitch and thermal sensitivity of the thermal imager are 17 μm and 0.5 °C, respectively. Its working spectrum ranges from 7.5 μm to 14 μm. The temperature range is −20 to 300 °C. The testing distance between the subject and the thermal imager is set to be 150 cm. Obtained thermal videos at a rate of 30 frame per second (fps) are imported into the data processing unit, and the Matlab R2014a (The Mathworks, Inc., Natick, MA, USA) is executed for the subsequent data analysis.

### 2.2. Thermal video database for breathing rate measurement

A thermal video database is established to validate the performance of various approaches for breathing rate measurement. A total of 11 subjects between the ages of 23 and 28 were invited to participate in the experiment. All participants involved in the experiments consented to be subjects. To create the proposed database, each participant was requested to sit on the chair and breathe for one minute, and simultaneously be recorded by the thermal imager. The thoracic belt is the standard instrument for breathing rate measurement, and it has to be strapped to the body of participant, which will make him or her uncomfortable and even painful. Therefore, in the current work, the ground truth breathing rate was counted by two dedicated and

**Table 2**
Summary of key differences between some previous studies using the thermal camera for breathing rate measurement.

| Study | Spatial resolution | Distance | Test environment |
|---|---|---|---|
| Fei and Pavlidis [27] | 640 × 512 pixels | ≈1.83 m | – |
| Pereira et al. [22,28] | 1024 × 768 pixels | ≈2.00 m | 22 °C and 50% |
| Lewis et al. [23] | 320 × 240 and 640 × 510 pixels | – | ≈21 °C |
| Abbas et al. [24] | – | < 1.5 m | – |
| Deepika et al. [25] | 1600 × 1200 pixels | 0.3–0.6 m | Room temperature |
| Bai et al. [26] | 1024 × 768 pixels | 0.02–5.33 m | – |
| Hu et al. [7,19] | 640 × 480 pixels | ≈1.5 m, 1–3 m | Room temperature |
| Basu et al. [18] | 320 × 240 pixels | – | 25 °C |

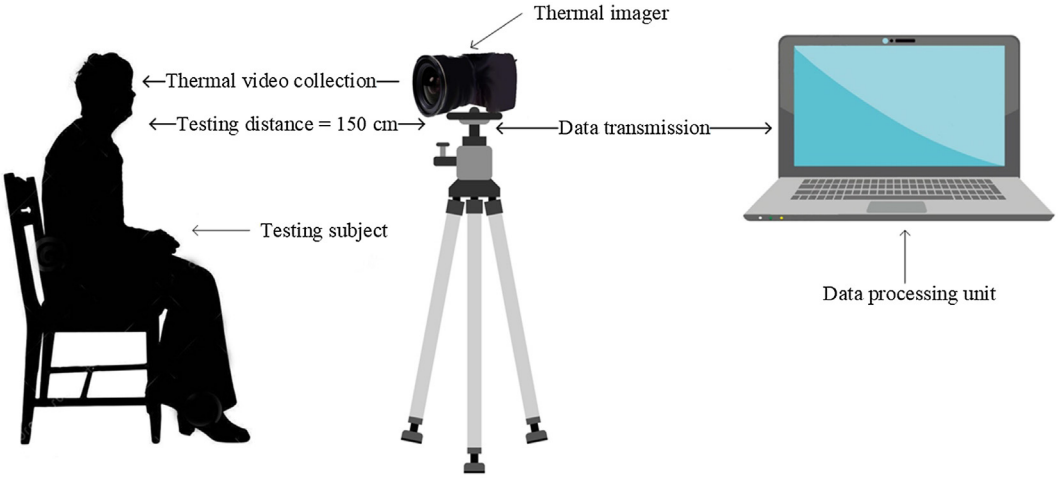


**Fig. 1.** Schematic illustration of experimental setup.

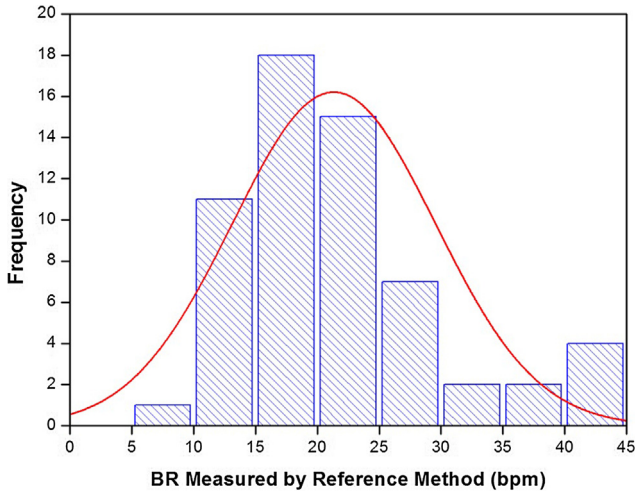


**Fig. 2.** Distribution of breathing rate in the proposed thermal video database.

qualified human observers, and then averaged for the subsequent analysis. Some participants were tested for several times, and therefore, there were 60 videos in the database. The distribution of breathing rate of these videos follows the Gaussian distribution (Fig. 2), allowing the examination of the robustness of the newly proposed system or method. This study was approved by the institutional review board (IRB) of the Shanghai Jiao Tong University and all participants provided full written informed consent. The individual in this manuscript has given written informed consent to publish these case details.

### 2.3. Data processing

Due to the principle of the thermal video in breathing rate estimation, the region of interest (ROI), including nostrils and mouth, is first manually confirmed in the first frame video. The off-the-shelf tracking algorithm – spatio-temporal context learning [29] is afterwards applied for tracking the ROI in the thermal video.

To form the thermal videos with different resolutions, the nearest-neighbor interpolation [30] is leveraged to resize the original video. The down-sampling rule is given as follows.

$$I_t = \mathrm{S}(I_t^{'}, r_x, r_y),\ t = 1, \cdots, \mathrm{T} \tag{1}$$

In equation, S is the scaling function and T is the number of video frame; $I_t$ and $I_t^{'}$represent the downsampled video and original video, respectively; $r_x$and$r_y$ denote the horizontal and vertical scaling ratio, respectively.

Thermal videos with various resolutions viz., 640 × 480, 512 × 384, 320 × 240, 192 × 144 and 64 × 48 were obtained using the nearest-neighbor interpolation (Fig. 3).

For each video, we can derive the average pixel intensity of ROI via the equation listed below.

$$\bar{s}(f) = \frac{1}{n} \sum_{i,j \in \boldsymbol{N}} s(i, j, f) \tag{2}$$

where s(i, j, $f$) is the pixel intensity of thermal image at pixel ($i$, $j$) and $f$th video frame; $\boldsymbol{N}$ is the vector of pixel coordinates in ROI and $n$ is its number.

In terms of BR extraction, the moving average filter with window size of 20 is first used to wipe off high frequency signals. Subsequently, the single-filtered signal is again smoothed by the moving average filter with window size of 50, and the double-filtered signal is generated by a

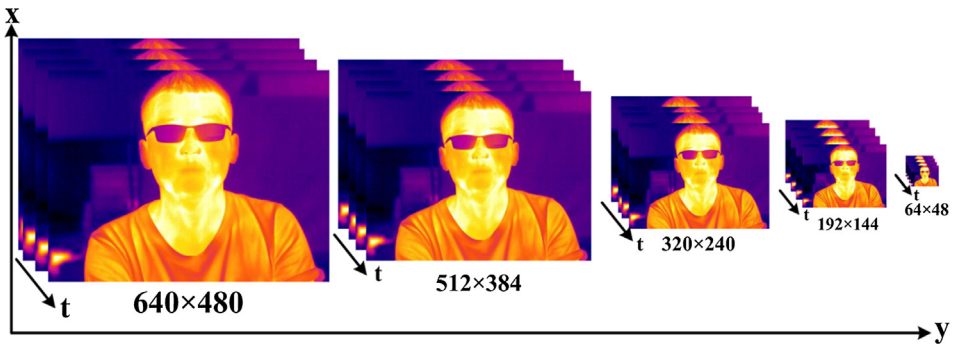


**Fig. 3.** The thermal videos with five different resolutions.

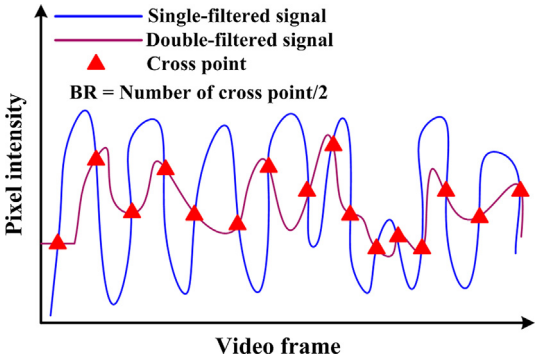


**Fig. 4.** Schematic diagram of algorithm for breathing rate calculation.

phase shift operation. As shown in Fig. 4, it can be observed that the BR can be computed from the number of cross points of two curves.

Two evaluation methodologies viz., Bland-Altman plot [31,32] and linear correlation analysis [33] are applied for assessing the influence of the thermal image resolutions on the performance of BR measurement.

## 3. Results

### 3.1. BR measurement using thermal video with original resolution

The Bland-Altman plot of thermal video with the resolution of 640 × 480 is demonstrated in Fig. 5(a) with the limits of agreements ranging from 2.599 bpm to 6.693 bpm and the mean of difference of 1.600 bpm. Most of scatter points located within the upper and lower 95% limits of agreement, and the nine testing points were in the line of perfect match. The above results indicated that the estimated BRs using the thermal imaging technique were in good agreement with the reference BRs.

The corresponding regression results of estimated and reference BRs are shown in Fig. 5(b). As shown in Fig. 5(b), the determination coefficient of 0.898 was found between the estimated and reference BRs, and nearly all testing points fell into the region between 95% confidence intervals. These results suggested that the performance of a thermal imaging system was extraordinarily good for remote BR measurement.

### 3.2. Effect of different resolutions on the performance of BR measurement

Fig. 6 shows the Bland-Altman plot of estimated BR derived from four down-sampled thermal videos and reference BR. The distances between the upper and lower limits of agreements were 10.595 bpm, 10.091 bpm, 15.168 bpm and 20.769 bpm for video resolutions of 512 × 384, 320 × 240, 192 × 144 and 64 × 48, respectively. From the above sub-section, the thermal video with original resolution viz., 640 × 480 achieved the distance of 4.094 bpm between two limits of agreements. This manifested that the thermal video with higher resolution, compared to those with the relatively lower resolutions, enabled the more excellent system performance for remote and unobtrusive BR measurement. By visual inspection of Figs. 5(a) and 6(a) as well as Fig. 6(b), the distributions of data points were basically similar to the thermal video with the resolutions of 640 × 480 and 512 × 384 as well as 320 × 240, respectively, indicating that the 320 × 240 resolution might give the comparable performance to the original resolution.

Fig. 7 demonstrates the results of linear correlation analysis for BR measured by the reference method and the thermal video with four different resolutions. As shown in Fig. 7, once the resolution was downsampled below 320 × 240, the system performance was seriously deteriorated ($R^2$ = 0.776 and 0.539 for 192 × 144 and 64 × 48, respectively). Based on the Fig. 5(b), Fig. 7(a) and (b), $R^2$ values ranged between 0.89 and 0.90 for three video resolutions, which were 640 × 480, 512 × 384 and 320 × 240. This finding is consistent with that in Bland-Altman analysis.

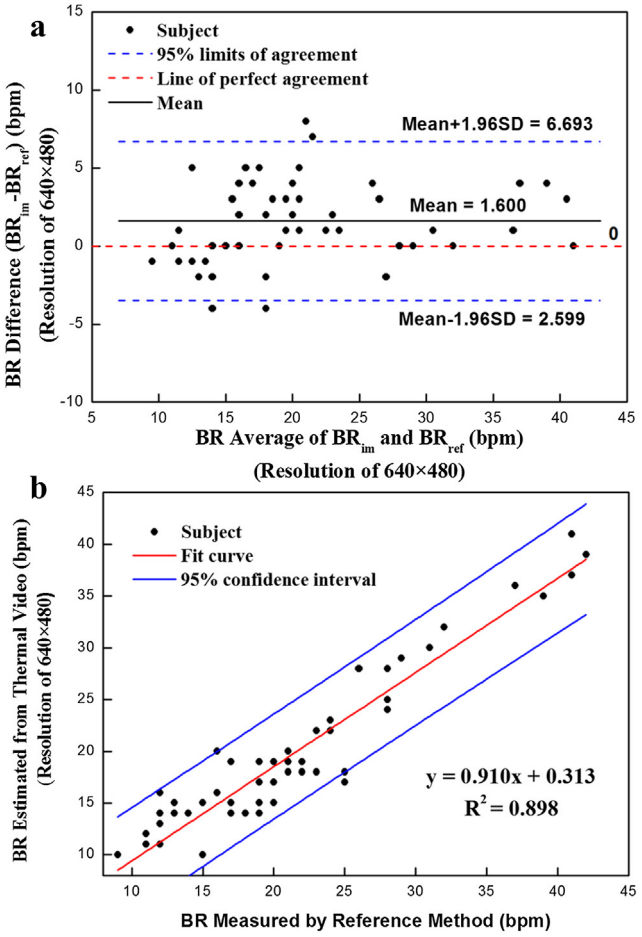


**Fig. 5.** Statistical analysis of BR measurement using thermal imaging system: (a) Bland-Altman plot ($N$ = 60) of the difference against average for BR via the reference method ($BR_{ref}$) and thermal imaging system ($BR_{im}$); and (b) correlation between estimated and reference BR ($N$ = 60). (Some testing points are overlapped in the plots).

## 4. Discussion

The above results revealed that the influence of resolution on the thermal imaging system performance for BR measurement was extremely significant for the relatively low resolutions. During the experiments, in order to reduce errors brought by ROI detection procedure, we select ROI manually in this study. The poor performance of resolution of 64 × 48 was attributed to the low tracking accuracy (Table 3). However, the comparable performance was observed at the resolution of 320 × 240 to the higher resolutions of 640 × 480 and 512 × 384 with the $R^2$ values of 0.900 versus 0.898 and 0.890. The possible reason for this might be that the higher resolution would introduce more uninformative or interferential factors into the analyzed signals, which in turn resulted in the performance deterioration.

From a practical point of view, the high resolution of thermal video may make the system more robust against many unknown interference factors, but may simultaneously increase hardware and computational cost. Due to the merits of non-contact optical imaging techniques, the application scope of the thermal camera in the physiological signal measurement will be wide in the future, ranging from the domestic health monitoring to the battlefield situation investigation. It is, therefore, important to select a camera resolution which is sufficiently

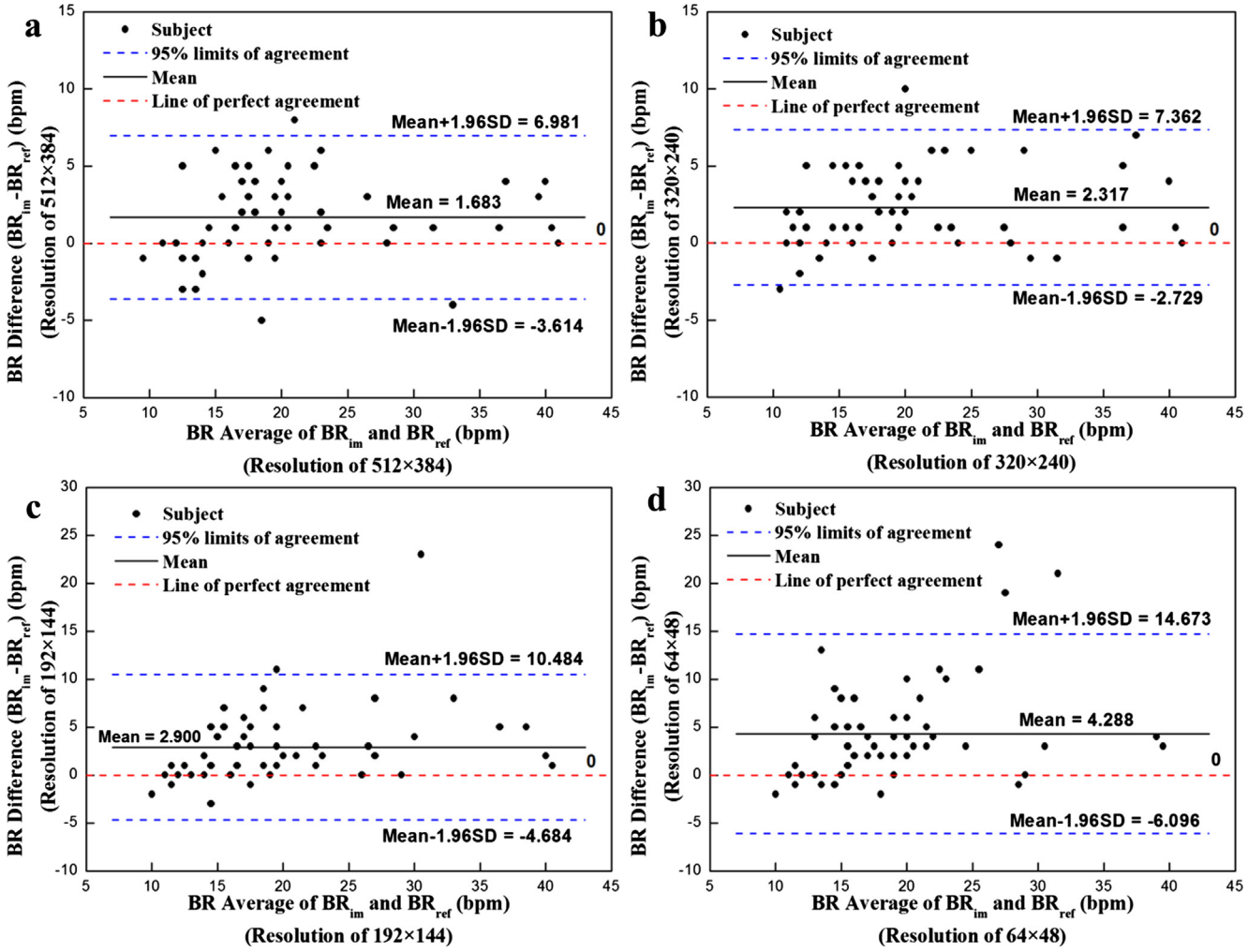


**Fig. 6.** Bland-Altman plot ($N = 60$) of the difference against average for BR using the reference method ($BR_{ref}$) and thermal videos ($BR_{im}$) with different resolutions.

suitable for a certain application scenario during the practical use. In this case, considering both computational cost and system performance, we can choose the resolution of 320 × 240 in some application scenarios (i.e. lie detection) where the measurement distance is approximately 1.5 m.

In terms of the application prospect, the thermal imaging system allows to measure the vital physiological signals in critical environments where is difficult or impossible to use contact sensors. For example, in clinical practice, the thermal imaging system can be used for burned patients and uncooperative persons who are in a coma or just an infant.

## 5. Conclusion

In conclusion, the thermal imaging technique was identified to be useful for remotely and unobtrusively measuring BR. In the Bland-Altman plot, distances between the upper and lower limits of agreements were 10.595 bpm, 10.091 bpm, 15.168 bpm and 20.769 bpm for video resolutions of 512 × 384, 320 × 240, 192 × 144 and 64 × 48, respectively. With respect to the linear correlation analysis, the determination coefficient ($R^2$) of 0.898, 0.890, 0.900, 0.776 and 0.539 had been observed for the resolutions of 640 × 480, 512 × 384, 320 × 240, 192 × 144 and 64 × 48, respectively. Overall, the effect of thermal video resolution on the system performance is extremely significant when the resolution is down-sampled below 320 × 240. Although the high resolution of thermal video may develop a more robust system for BR measurement, it may also increase hardware and computational cost as well as introduce other unknown error sources. Hence, in the application perspective, we should select the suitable video resolution by balancing the system performance and the cost. In this case, the resolution of 320 × 240 can be selected in some application scenarios where the measurement distance is approximately 1.5 m.

In clinical terms, the clinical requirements for breathing rate measurement require to be considered in the future study. How the image resolution affects the accuracy of on-the-move BR measurements in various application scenarios such as moving individuals in airport? This should be studied in future. Furthermore, the further studies have to give some explicit application cases for the issue of the cost in the resolution of thermal sensors.

## Acknowledgments

The authors thank all the volunteers who agreed to participate in this study. Also, the authors would also like to thank Ms. Huijing Huang for providing assistance with the English language revision.

## Grant/funding support

The authors would like to acknowledge the China Postdoctoral Science Foundation funded project (No. 2016M600315), the Equipment Pre-research Joint Research Program of Ministry of Education (No. 6141A020223), the financial support from the National Science Foundation of China under Grant (61521062, 61527804 and

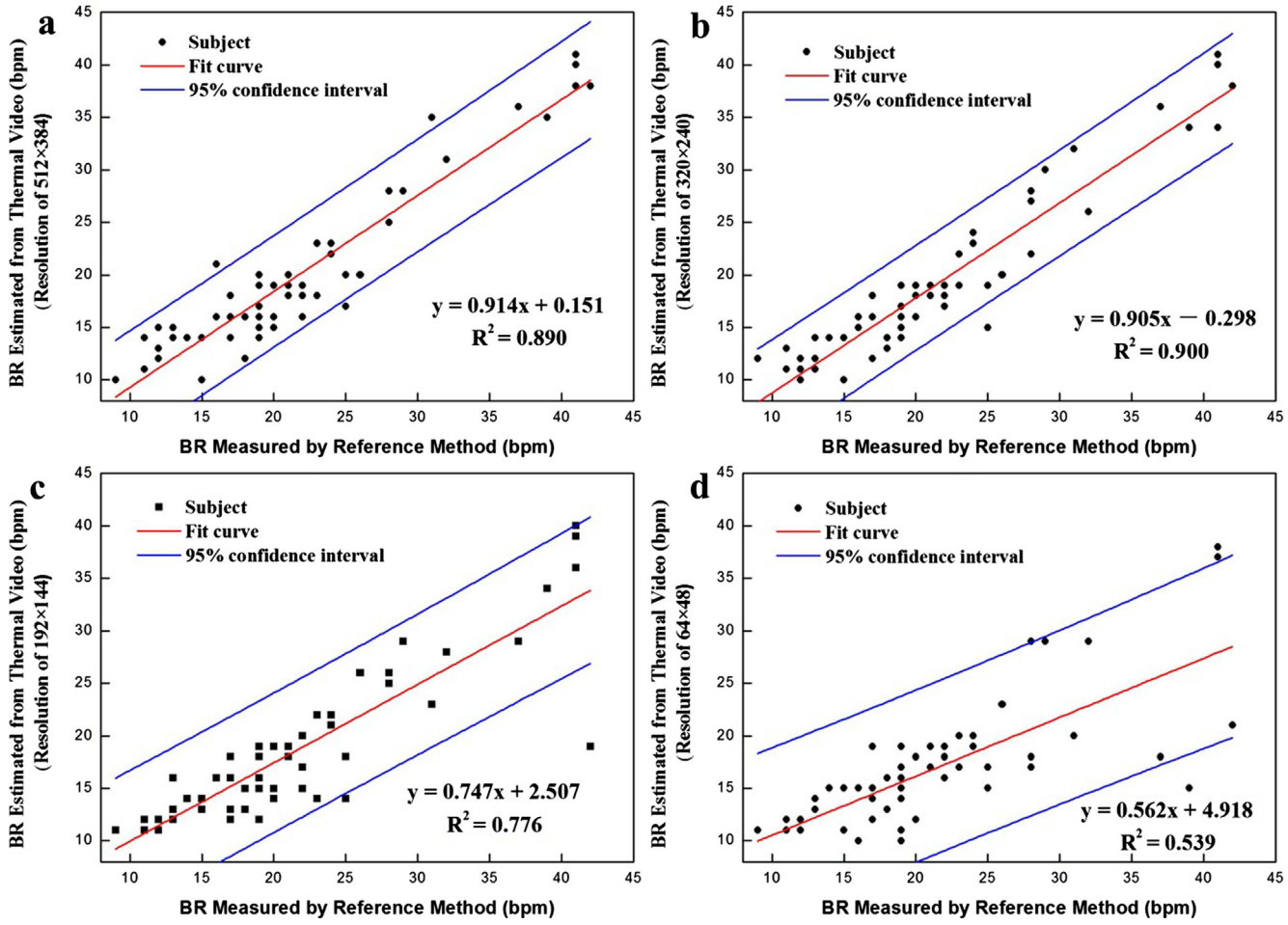


**Fig. 7.** Linear correlation analysis of BR measured by the reference method and thermal video with different resolutions.

**Table 3**
Tracking accuracies of ROI in the thermal video with different resolutions.

| Resolution | No. of thermal video | No. of successful tracking | Accuracy (%) |
|---|---|---|---|
| 640 × 480 | 60 | 57 | 95% |
| 512 × 384 | | 56 | 93% |
| 320 × 240 | | 53 | 88% |
| 192 × 144 | | 52 | 87% |
| 64 × 48 | | 32 | 53% |

61471234), and the Science and Technology Commission of Shanghai Municipality (15DZ0500200 and 17DZ1205602).

## Conflict of interest

The authors declare that they do not have any conflicts of interest.

## Appendix A. Supplementary material

Supplementary data associated with this article can be found, in the online version, at https://doi.org/10.1016/j.infrared.2018.05.026.

## References

[1] O.K. Nguyen, A.N. Makam, C. Clark, S. Zhang, B. Xie, F. Velasco, R. Amarasingham, E.A. Halm, Vital signs are still vital: instability on discharge and the risk of post-discharge adverse outcomes, J. Gen. Intern. Medi. 32 (2017) 42–48.
[2] S.C. Gandevia, D.K. Mckenzie, Respiratory rate: the neglected vital sign, Med. J. Aus. 188 (2008) 657–659.
[3] B. Brock, S. Kamysek, J. Silz, P. Trefz, J.K. Schubert, W. Miekisch, Monitoring of breath VOCs and electrical impedance tomography under pulmonary recruitment in mechanically ventilated patients, J. Breath Res. 11 (2017) 016005.
[4] S. Nahar, N. Tran, L. Ren, O. Kilic, A.E. Fathy, Through-wall detection of human breathing rate using compressive sensing technique, in: 2017 IEEE Radio and Wireless Symposium (RWS), 2017, pp. 104–107.
[5] P. Arlotto, M. Grimaldi, R. Naeck, J.-M. Ginoux, An ultrasonic contactless sensor for breathing monitoring, Sensors 14 (2014) 15371.
[6] S.D. Min, K.K. Jin, S.S. Hang, Y.H. Yun, Noncontact respiration rate measurement system using an ultrasonic proximity sensor, IEEE Sens. J. 10 (2010) 1732–1739.
[7] M.H. Hu, G.T. Zhai, D. Li, Y.Z. Fan, X.H. Chen, X.K. Yang, Synergetic use of thermal and visible imaging techniques for contactless and unobtrusive breathing measurement, J. Biomed. Opt. 22 (2017) 36006.
[8] L. Tarassenko, M. Villarroel, A. Guazzi, J. Jorge, D.A. Clifton, C. Pugh, Non-contact video-based vital sign monitoring using ambient light and auto-regressive models, Physiol. Measur. 35 (2014) 807.
[9] D. Shao, Y. Yang, C. Liu, F. Tsow, H. Yu, N. Tao, Noncontact monitoring breathing pattern, exhalation flow rate and pulse transit time, IEEE Trans. Biomed. Eng. 61 (2014) 2760–2767.
[10] H. Aoki, Y. Takemura, K. Mimura, M. Nakajima, Development of non-restrictive sensing system for sleeping person using fiber grating vision sensor, in: International Symposium on Micromechatronics and Human Science, 2001, pp. 155–160.
[11] W. Daw, Medical Devices for Measuring Respiratory Rate in Children: A Review, 2016.
[12] A.D. Droitcour, T.B. Seto, B.K. Park, S. Yamada, A. Vergara, C.E. Hourani, T. Shing, A. Yuen, V.M. Lubecke, O. Boriclubecke, Non-contact respiratory rate measurement validation for hospitalized patients, in: Engineering in Medicine and Biology Society, 2009. EMBC 2009 International Conference of the IEEE, 2009, pp. 4812.
[13] L. Scalise, P. Marchionni, I. Ercoli, Non-contact laser-based human respiration rate measurement, 1364, 2011, 149–155.
[14] B.A. Reyes, N. Reljin, Y. Kong, Y. Nam, S. Ha, K.H. Chon, Towards the development of a mobile phonopneumogram: automatic breath-phase classification using smartphones, Ann. Biomed. Eng. 44 (2016) 1–14.
[15] Y. Nam, Y. Kong, B. Reyes, N. Reljin, K.H. Chon, Monitoring of heart and breathing rates using dual cameras on a smartphone, Plos One 11 (2016) e0151013.
[16] F. Centonze, M. Schätz, A. Procházka, J. Kuchyňka, O. Vyšata, P. Cejnar, M. Vališ, Feature extraction using MS Kinect and data fusion in analysis of sleep disorders, in:

International Workshop on Computational Intelligence for Multimedia Understanding, 2015, pp. 1–5.
[17] J. Lee, M. Hong, S. Ryu, Sleep monitoring system using kinect sensor, Int. J. Distrib. Sens. Netw. (2015) 1–9.
[18] A. Basu, A. Routray, R. Mukherjee, S. Shit, Infrared imaging based hyperventilation monitoring through respiration rate estimation, Infrared Phys. Tech. 77 (2016) 382–390.
[19] M. Hu, G. Zhai, D. Li, Y. Fan, H. Duan, W. Zhu, X. Yang, Combination of near-infrared and thermal imaging techniques for the remote and simultaneous measurements of breathing and heart rates under sleep situation, Plos One 13 (2018) e0190466.
[20] M. Yang, Q. Liu, T. Turner, Y. Wu, Vital sign estimation from passive thermal video, in: Computer Vision and Pattern Recognition, 2008. CVPR 2008. IEEE Conference on, 2008, pp. 1–8.
[21] A.K. Abbas, K. Heimann, K. Jergus, T. Orlikowsky, S. Leonhardt, Neonatal non-contact respiratory monitoring based on real-time infrared thermography, BioMed. Eng. OnLine 10 (2011) 93.
[22] C.B. Pereira, X. Yu, M. Czaplik, R. Rossaint, V. Blazek, S. Leonhardt, Remote monitoring of breathing dynamics using infrared thermography, Biomed. Opt. Exp. 6 (2015) 4378–4394.
[23] G.F. Lewis, R.G. Gatto, S.W. Porges, A novel method for extracting respiration rate and relative tidal volume from infrared thermography, Psychophysiology 48 (2011) 877.
[24] A.K. Abbas, K. Heiman, T. Orlikowsky, S. Leonhardt, Non-Contact respiratory monitoring based on real-time IR-thermography, Ifmbe Proc. 25 (2009) 1306–1309.
[25] C.L. Deepika, A. Kandaswamy, G. Pradeepa, An efficient method for detection of inspiration phase of respiration in thermal imaging, 2016.
[26] Y.W. Bai, C.L. Tsai, S.C. Wu, Design of a breath detection system with multiple remotely enhanced hand-computer interaction devices, in: 2012 IEEE 16th International Symposium on Consumer Electronics, 2012, pp. 1–5.
[27] J. Fei, I. Pavlidis, Thermistor at a distance: unobtrusive measurement of breathing, IEEE Trans. Biomed. eng. 57 (2010) 988.
[28] P.C. Barbosa, X. Yu, M. Czaplik, V. Blazek, B. Venema, S. Leonhardt, Estimation of breathing rate in thermal imaging videos: a pilot study on healthy human subjects, J. Clin. Monit. Comput. 31 (2017) 1241–1254.
[29] K. Zhang, L. Zhang, Q. Liu, D. Zhang, M.H. Yang, Fast visual tracking via dense spatio-temporal context, Learning 8693 (2014) 127–141.
[30] N. Jiang, L. Wang, Quantum image scaling using nearest neighbor interpolation, Quantum Infor. Process. 14 (2015) 1559–1571.
[31] A. Carkeet, Exact parametric confidence intervals for Bland-Altman limits of agreement, Opto. Vision Sci. Offic. Publi. Am. Academy Opto. 92 (2015) 71–80.
[32] L.S. Nawarathna, P.K. Choudhary, Measuring agreement in method comparison studies with heteroscedastic measurements, Statist. Med. 32 (1999) 5156–5171.
[33] M.H. Hu, Q.L. Dong, B.L. Liu, U.L. Opara, Prediction of mechanical properties of blueberry using hyperspectral interactance imaging, Postharvest Biol. Tech. 115 (2016) 122–131.